



Solutions to micromagnetic standard problem No. 2 using square grids

L. Lopez-Diaz, O. Alejos, L. Torres, and J. I. Iniguez

Citation: *Journal of Applied Physics* **85**, 5813 (1999); doi: 10.1063/1.369928

View online: <http://dx.doi.org/10.1063/1.369928>

View Table of Contents: <http://scitation.aip.org/content/aip/journal/jap/85/8?ver=pdfcov>

Published by the [AIP Publishing](#)

Articles you may be interested in

[The effect of interelement dipole coupling in patterned ultrathin single crystal Fe square arrays](#)

J. Appl. Phys. **109**, 033913 (2011); 10.1063/1.3544348

[Magnetic properties enhancement of Nd₂Fe₁₄B/ \$\alpha\$ -Fe nanocomposites with a combined addition of Cu and Ti](#)

J. Appl. Phys. **93**, 1199 (2003); 10.1063/1.1530368

[Comparison of magnetostatic field calculation methods on two-dimensional square grids as applied to a micromagnetic standard problem](#)

J. Appl. Phys. **85**, 5816 (1999); 10.1063/1.369929

[Magnetic phase diagram of ultrathin Co/Si\(111\) film studied by surface magneto-optic Kerr effect](#)

Appl. Phys. Lett. **74**, 1311 (1999); 10.1063/1.123534

[Micromagnetic computational standard problem \(abstract\)](#)

J. Appl. Phys. **81**, 5242 (1997); 10.1063/1.364955

AIP | Chaos

CALL FOR APPLICANTS

Seeking new Editor-in-Chief

Solutions to micromagnetic standard problem No. 2 using square grids

L. Lopez-Diaz^{a)}

Departamento de Fisica Aplicada, Universidad de Salamanca, Salamanca E-37071, Spain

O. Alejos

Departamento de Electricidad y Electronica, Universidad de Valladolid, Valladolid E-47071, Spain

L. Torres and J. I. Iniguez

Departamento de Fisica Aplicada, Universidad de Salamanca, Salamanca E-37071, Spain

Solutions to micromagnetic standard problem No. 2 are presented in this article and the main features of the computational techniques used are discussed. Values of coercivity and remanence have been obtained in the range $0.8 < d/l_{\text{ex}} < 20.0$. A continuous transition from uniform to nonuniform rotation is observed leading to a steady decrease in the coercivity as the ratio between the scaled geometry and the exchange length is increased. A sharp transition in the remanent states is found at $d/l_{\text{ex}} = 9.0$. The nonuniform reversal mechanism is discussed and is found to consist on transitions between in-plane S-shaped patterns. The results are interpreted qualitatively. © 1999 American Institute of Physics. [S0021-8979(99)41008-4]

I. INTRODUCTION

Several micromagnetic standard problems have been proposed by the micromagnetic modeling activity group (μMAG).¹ The aim of this initiative is to come up with a set of standard problems for which a general agreement on the solution is reached, allowing the researchers working on numerical micromagnetics to compare computational techniques and identify problems with their code.

This article deals with standard problem No. 2. According to the specifications,¹ a rectangular thin film of length L , width d , and thickness t is considered. If crystalline anisotropy is neglected and the geometry is fixed, scaling of the micromagnetic equilibrium equation yields a hysteresis loop which depends only on the scaled geometry to the exchange length when expressed as M/M_s versus H/H_m , where $H_m = 4\pi M_s$ (cgs emu will be used). The exchange length is $l_{\text{ex}} = (A/K_m)^{1/2}$, where A is the exchange stiffness constant and K_m is a magnetostatic energy density $K_m = 2\pi M_s^2$. Applying the external field in the $[111]$ direction and setting the geometry of the system to $L/d = 5.0$ and $t/d = 0.1$, an investigation of the reversal modes for different values of d/l_{ex} is proposed.

II. COMPUTATIONAL TECHNIQUES

In order to solve the micromagnetic equilibrium equation for the system, the film is discretized in a two-dimensional (2D) square mesh, while the magnetization is allowed to rotate in three dimensional (3D). Four different methods have been used to relax the system: Labonte,² Berkov,³ Landau–Lifschitz–Gilbert (LLG),⁴ and the conjugate gradient method (CGM).⁵ It was found that they all converged to the same solutions and that CGM was the fastest in all cases. In particular, for small d/l_{ex} the problem becomes stiff and CGM is many times faster than the rest of the methods. It has already been pointed out that CGM can

be very efficient handling stiff problems.⁴ The four-neighbor dot product representation⁶ was chosen for the exchange energy, whereas the demagnetizing field was calculated in the middle plane ($z=0$) of the film assuming a constant magnetization in each cell. The convergence criterion for terminating the iterations at a given field was $|\mathbf{m} \times \mathbf{h}_{\text{eff}}| < 10^{-5}$ in every computational cell, where $\mathbf{m} = \mathbf{M}/M_s$ and $\mathbf{h}_{\text{eff}} = \mathbf{H}_{\text{eff}}/M_s$.⁴ Further decreases in the maximum torque yielded no noticeable change in the results. The cell size Δ was chosen to be several times smaller than $l_{\text{ex}}\Delta/l_{\text{ex}} \leq 0.25$. It was found that, for small values of d/l_{ex} , the shape of the hysteresis loop as the field approaches coercivity depends significantly on the value of Δ . In those cases, loops were calculated for several Δ and an extrapolation to $\Delta=0$ was carried out for each d/l_{ex} as it will be shown later.

Starting from complete saturation, hysteresis loops were computed as a series of equilibrium states for the corresponding sequence of applied fields. The interval $-10 < H/H_m < 10$ was covered with an adaptive step size ranging from 1 to 0.001 (smaller steps were taken when the rate in the change of magnetization was higher). It was found that the equilibrium state at a given field is independent of how the field was stepped previously, provided that the initial state is the same.

III. RESULTS

Hysteresis loops have been computed in the range $0.8 < d/l_{\text{ex}} < 20.0$. The results are presented in Fig. 1, where the variation of coercivity (H_c/H_m) and remanence [M_r^x , M_r^y , and $M_r^{[111]} = (M_r^x + M_r^y + M_r^z)/3^{1/2}$] with d/l_{ex} is plotted. The values of H_c/H_m in Fig. 1(a) have been obtained by extrapolating the computed values to $\Delta=0$ with a second order curve. Typical extrapolations are presented in Fig. 2. However, the extrapolation could not be carried out for $d/l_{\text{ex}} < 4.0$ since no clear convergence was achieved. Consequently, the corresponding values are not plotted in Fig. 1(a). Although no convergence was achieved for the remanence

^{a)}Electronic mail: Lld@gugu.usal.es

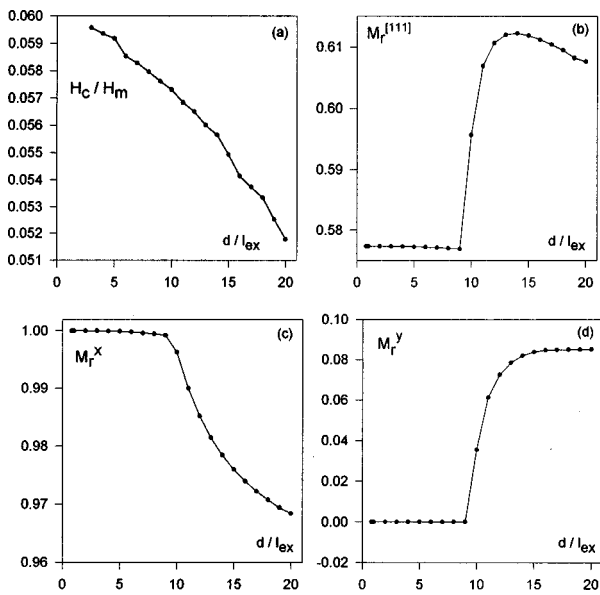


FIG. 1. Variation of coercivity (a) and remanence (b)–(d) with d/l_{ex} .

either, its dependence on Δ is negligible compared to its variation with d/l_{ex} and the computed values for a discretization size of $\Delta/l_{ex}=4$ have been plotted in all cases.

As shown in Fig. 1(a), a steady decrease in the coercivity is obtained, adding up to a 13% reduction in H_c/H_m in the range considered. A single nonuniform reversal mode is found, which will be discussed in the next section. The magnetization configurations at remanence are found to lie in the xy plane in all cases and a sharp transition is found for d/l_{ex} between 9.0 and 10.0. The remanent state for $0.8 \leq d/l_{ex} \leq 9.0$ is basically uniform along the x axis, whereas for $9.0 \leq d/l_{ex} \leq 20.0$ an S-shaped pattern [shown in Fig. 4(a)] is found.

IV. DISCUSSION

The results presented above are interpreted and the reversal mechanism is discussed in this section. The qualitative features of the hysteresis curves are the same throughout the range considered. Three well defined magnetization patterns

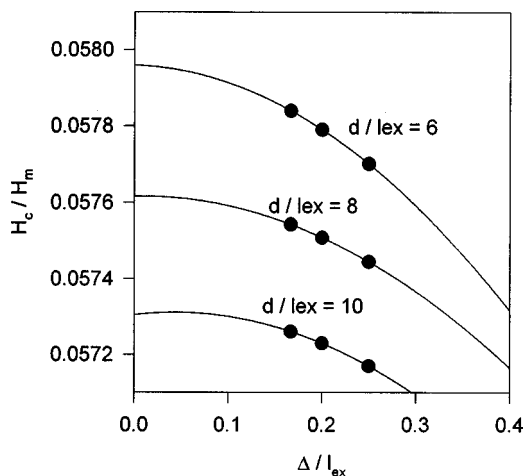


FIG. 2. Typical extrapolations to $\Delta=0$ in the calculation of the H/H_m .

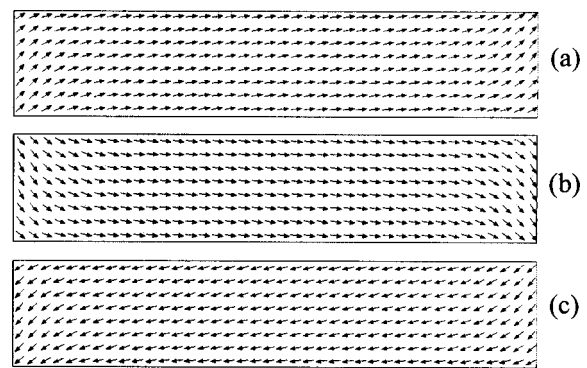


FIG. 3. Magnetization patterns found in the reversal mode: S-UR (a), S-DR (b), and S-DL (c) configurations. The plots correspond to $d/l_{ex}=12.0$.

are found in the reversal process. They are represented in Fig. 3. These configurations consist on deviations from a uniform magnetization at the edges of the sample that reduce the magnetostatic energy of the system. They will be referred generically as S-shaped patterns and we will distinguish among them by the direction towards which the magnetization vector is pointing at the edges of the sample: up right (S-UR), down right (S-DR), and down left (S-DL) in Figs. 3(a)–3(c), respectively. Typical hysteresis loops can be observed in Figs. 4 and 5, where the different regions are labeled with the corresponding magnetization pattern. In Fig. 4, the curve of the magnetization along the field axis is represented for the $d/l_{ex}=20.0$ case. In Fig. 5 the descending branches for different projections of \mathbf{M} are plotted for $d/l_{ex}=10.0$.

Although saturation along the field axis is achieved for high fields (typically $H/H_m=10$ is required for 99% saturation), the range $-0.1 < H/H_m < 0.1$ is where most of the magnetization reversal takes place. As can be seen in Fig. 5, M_z is very small in this region and therefore, we are dealing with an in-plane switching mode. Starting from positive satu-

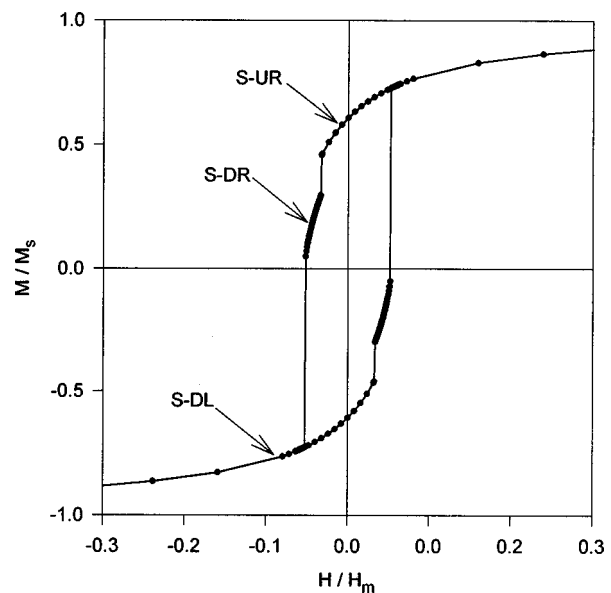


FIG. 4. Hysteresis loop for $d/l_{ex}=20.0$. $M^{[111]}/M_s$ is plotted in the vertical axis.

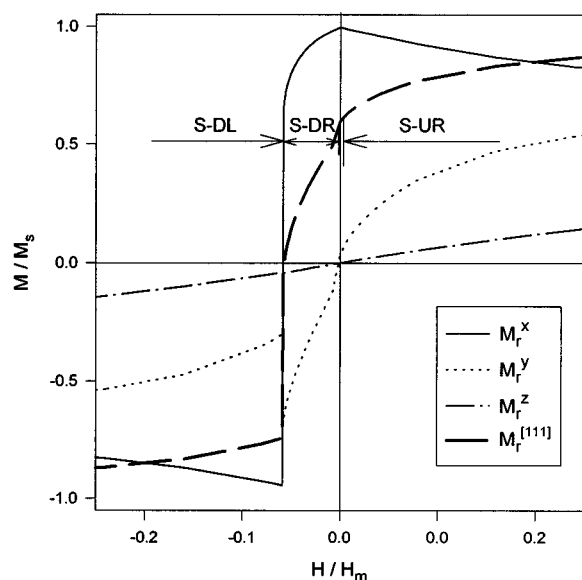


FIG. 5. Descending branch of hysteresis loop for $d/l_{\text{ex}} = 12.0$. Different projections of \mathbf{M} are plotted.

ration, the out-of-plane component vanishes and a S-UR configuration is formed as the field is decreased. After that, a transition from S-UR to S-DR takes place. This transition can be recognized in Fig. 5 at $H/H_m \approx 0$, where M_y switches from a positive to a negative value and the slope of the M_x curve changes from a negative to a positive value. Later on, an irreversible transition from state S-DR to state S-DL occurs, as can be noticed in Fig. 5 by the big jump in the M_x curve. If the field is decreased further, the magnetization evolves reversibly towards negative saturation.

As d/l_{ex} gets smaller, the transition from S-UR to S-DR moves to the right in the hysteresis curve and becomes more gradual, as can be noted by comparing Figs. 4 and 5. This fact explains the transition in the remanent states observed in Fig. 1. For $d/l_{\text{ex}} \geq 10.0$ the transition occurs at a negative field and consequently, the remanent state corresponds to a S-UR configuration, characterized by a positive M_y . However, for $d/l_{\text{ex}} \leq 9.0$ the transition starts at a positive field and the remanent state corresponds to an intermediate state in

this transition, which is basically a uniform configuration along the horizontal axis ($M_x/M_s \approx 1$). On the contrary, the transition from S-DR to S-DL is more abrupt and it moves to the left when the size of the film is reduced, which explains the increase in the coercivity observed in Fig. 1(a).

To sum up, as the scaled geometry of the system is reduced, the deviation from uniform magnetization is reduced and consequently, the energy barrier from S-UR to S-DR disappears, whereas the barrier from S-DR to S-DL increases. Therefore, a continuous transition from the reversal mechanism that has been discussed to uniform rotation is found.

V. CONCLUSIONS

Solutions for the micromagnetic standard problem No. 2 have been presented in the $0.8 < d/l_{\text{ex}} < 20.0$ range. A continuous transition from uniform to nonuniform rotation is observed leading to a steady decrease in the coercivity as the ratio between the scaled geometry and the exchange length is increased. The nonuniform reversal mode consists on transitions between in-plane S-shaped patterns and no vortex modes have been found in the range considered.

An increasing dependence of the solutions on the discretization is observed as d/l_{ex} becomes smaller and an extrapolation to an infinitely small discretization is carried out. No convergence for the computed values of the coercivity is obtained in the range $d/l_{\text{ex}} < 4.0$.

ACKNOWLEDGMENT

This work has been supported by the Castilla y Leon Government under Project No. SA55/99.

¹ See <http://www.ctcms.nist.gov/~rdm/mumag.org.html>

² A. E. Labonte, J. Appl. Phys. **40**, 2450 (1969).

³ D. V. Berkov, K. Ramst ock, and A. Hubert, Phys. Status Solidi A **137**, 207 (1993).

⁴ L. Lopez-Diaz, J. Eicke, and E. Della Torre, IEEE Trans. Magn. (to be published).

⁵ W. H. Press, S. A. Teukolsky, W. T. Wetterling, and B. P. Flannery, *Numerical Recipes in Fortran* (Cambridge University Press, Cambridge, 1996).

⁶ M. J. Donahue and R. D. McMichael, Physica B **233**, 272 (1997).